Equatorial Waves and Air–Sea Interaction in the Boreal Summer Intraseasonal Oscillation

SUSAN KEMBALL-COOK* AND BIN WANG+

Department of Meteorology, School of Ocean and Earth Science and Technology, University of Hawaii at Manoa, Honolulu, Hawaii

(Manuscript received 29 February 2000, in final form 14 August 2000)

ABSTRACT

A composite study of the life cycle of the boreal summer intraseasonal oscillation (BSISO) was performed using data from the National Centers for Environmental Prediction–National Center for Atmospheric Research reanalysis and National Oceanic and Atmospheric Administration polar-orbiting satellites. Because of pronounced differences in their climatologies, the boreal summer periods May–June (MJ) and August–October (AO) were composited separately. Characteristics of the BSISO life cycle common to MJ and AO were initiation and eastward propagation of the convective anomaly over the Indian Ocean, followed by poleward propagation, with the northward-moving branch having greater amplitude than the southward-moving branch. The transition of convection from the Indian Ocean to the western Pacific occurred next, followed by dissipation of the current cycle and initiation of the subsequent cycle. The MJ and AO life cycles were found to have several significant differences. The MJ shows strong eastward movement of convection along the equator in both the Indian and western Pacific Oceans. Convection in AO has a weaker eastward-propagating signal along the equator and displays a discontinuous jump from the Indian Ocean to the western Pacific. In marked contrast to MJ, AO shows strong northwestward propagation of convection in the western Pacific during the latter half of the BSISO life cycle. The change in the BSISO life cycle from MJ to AO reflects the seasonal shift in the distributions of vertical wind shear and low-level specific humidity from early to late summer. Rossby waves emitted by equatorial convection play a critical role in the BSISO in both the Indian and western Pacific Oceans. These waves are instrumental in the northward propagation of convection in MJ and AO. Both MJ and AO composites suggest that air–sea interactions are present in the BSISO, fostering both eastward and northward propagation of convective anomalies in the Indian Ocean and in the western Pacific. The complexity and pronounced seasonal dependence of the BSISO reflected in the composites suggest that its simulation is a rigorous test for general circulation models.

1. Introduction

The tropical intraseasonal oscillation (ISO) exhibits pronounced seasonality in its frequency (Hartmann et al. 1992), intensity (Madden 1986), and movement (Wang and Rui 1990). The dominant oscillation period in the Indian Ocean is about 50 days during boreal winter and about 35 days in boreal summer (Hartmann et al. 1992). During boreal summer, the eastward-propagating Madden–Julian oscillation (MJO) mode (Madden and Julian 1971, 1972) is notably weaker than in boreal winter (Wang and Rui 1990; Hendon and Salby 1994). In boreal summer, the ISO is characterized by prominent northward propagation in the Indian summer monsoon region (Yasunari 1979; Krishnamurti and Subrahmanyam 1982; Hartmann and Michelsen 1989) and over the western North Pacific (Chen and Murakami 1988). Over the off-equatorial western Pacific, intraseasonal convective activity exhibits prevailing westward propagation (with a period of 20–30 days) from July to October (Murakami et al. 1984; Nitta 1987; Wang and Xie 1997). The ISO is considerably more complex during boreal summer than in winter due to the coexistence of multiple (eastward, northward, westward) low-frequency propagation modes and the interactions among them.

The complexity of the boreal summer ISO (BSISO) may arise in part from its vigorous interaction with the pronounced seasonal cycle associated with the powerful Asian–Australian monsoon system. As illustrated by Webster et al. (1998), the Asian summer monsoon affects planetary-scale motion through its lateral and transverse monsoon and Walker circulations. The ver-

* Current affiliation: Lawrence Berkeley National Laboratory, Berkeley, California.

+ Current affiliation: Department of Meteorology and International Pacific Research Center,# University of Hawaii at Manoa, Honolulu, Hawaii.

The International Pacific Research Center is sponsored in part by the Frontier Research System for Global Change.

Corresponding author address: Dr. Susan Kemball-Cook, Earth Sciences Division, Lawrence Berkeley National Laboratory, MS 90-1116, 1 Cyclotron Rd., Berkeley, CA 94720.
E-mail: srkemball-cook@lbl.gov

tical shear of the monsoon flows, through the coupling of baroclinic and barotropic components of atmospheric motion, has fundamental impacts on the vertical structure, growth, and propagation of moist equatorial Rossby waves (Wang and Xie 1996; Xie and Wang 1996), which have been shown (Wheeler and Kiladis 1999) to be important in the ISO. Numerical experiments by Li and Wang (1994) demonstrate the impact of the seasonal variation of SST and associated moisture on the seasonality of the ISO. The model results of Wang and Xie (1997) indicate that the background circulation and the underlying distribution of SST and boundary layer moist static energy strongly regulate the behavior of moist equatorial waves and contribute to the creation of the pronounced regional characteristics of the BSISO.

The complex behavior of the BSISO may also arise from its interaction with underlying ocean mixed layer thermodynamics and land surface processes. Although the ISO in the surface latent heat fluxes and SST was observed more than a decade ago (Krishnamurti et al. 1988), it was not until after the Tropical Ocean and Global Atmosphere Coupled Ocean–Atmosphere Response Experiment (TOGA COARE) that air–sea heat and momentum exchanges on intraseasonal timescales were documented with confidence. The coupled structure of the boreal winter MJO mode and the underlying ocean has been described in detail (e.g., Zhang 1996; Jones and Weare 1996; Lin and Johnson 1996; Hendon and Glick 1997, etc.). The intraseasonal variability of surface fluxes induced by the MJO has profound impacts on the intraseasonal variation of SST (Lau and Sui 1997; Jones et al. 1998; Shinoda et al. 1998; Shinoda and Hendon 1998). Convection-generated SST gradients have been shown to play an important role in cloud cluster development and propagation (Flatau et al. 1997). These observational analyses have stimulated a number of theoretical and modeling studies.

The theoretical analysis of Wang and Xie (1998) showed that air–sea thermodynamic interaction through wind–evaporation and cloud–radiation feedback is conducive to coupled unstable modes on intraseasonal timescales in the warm pool. Using the Goddard Laboratory for Atmospheres GCM coupled with a swamp ocean mixed layer. Waliser et al. (1999) demonstrated that an interactive SST facilitates a better simulation of the MJO. The improvements included increased MJO variability, reduced eastward phase speed in the Eastern Hemisphere, and increased seasonality.

Numerical modeling of the ISO is in its infancy. Simulation of the rainfall climatology and variability over the monsoon region and the warm waters of the Indian and Pacific Oceans has been a great challenge for coupled GCMs. Even state-of-the-art coupled GCMs have considerable difficulty in accurately representing the Pacific annual cycle (Mechoso et al. 1995; Li and Hogan 1999) and the mean monsoon circulation (Hoskins and Rodwell 1995). Common model weaknesses in reproducing the MJO were documented by Slingo et al. (1996). The performance of atmospheric GCMs in simulating the BSISO has not been systematically compared with observations. It should be noted that direct observations of the interaction between the BSISO and the ocean mixed layer in the Indian monsoon region are rare.

Lack of understanding of the essential physics of the BSISO is a major obstacle for further improvement of numerical models and their simulation of the ISO. The dynamics of northward propagation in the Indian Ocean and westward propagation in the western Pacific may differ fundamentally from the eastward equatorial propagation prominent in the MJO. Revealing the physical processes responsible for the BSISO will not only advance our understanding of the mechanisms of the tropical ISO but will improve our capability for predicting the tropical ISO and the intraseasonal variability of the global-scale boreal summer circulation.

The aim of this study is to improve our understanding of the BSISO by documenting its composited life cycle. Our general hypotheses are 1) that air–sea interactions play a role in the northward and westward propagation of the BSISO structures and in its reinitiation in the Indian Ocean; 2) that the ISO has a different character during early and late summer due to the change in the mean flow.

In section 2, we describe the datasets and compositing method used in this study. The life cycle of the BSISO during early and late summer is presented in section 3. The roles played by Rossby waves and air–sea interactions are discussed in sections 4 and 5, respectively. Section 6 is a summary of the results, and section 7 gives conclusions and directions for further study.

2. Data and method

The datasets used to form the composite life cycle of the BSISO are interpolated daily average maps of outgoing longwave radiation (OLR) from the National Oceanic and Atmospheric Administration (NOAA) polar-orbiting satellites (Liebmann and Smith 1996) and daily average fields from the National Centers for Environmental Prediction–National Center for Atmospheric Research (NCEP–NCAR) reanalysis (Kalnay et al. 1996). The NCEP–NCAR fields used were those expected to show the basic dynamical structure of the BSISO (200-mb and 850-mb winds, vertical pressure velocity at 500 mb) and highlight air–sea interactions (surface downward shortwave radiative flux, surface latent heat flux, skin temperature, air temperature, specific humidity, and geopotential height). Fifteen years of data were used, extending from 1983 to 1997.

Both the OLR and the Reanalysis fields were filtered in the same manner using a bandpass filter that retains variability in the 10–100-day band. The annual cycle and its first three harmonics and the interannual variability were removed using the method of Rui and Wang (1990). Then, a running pentad mean was applied to the

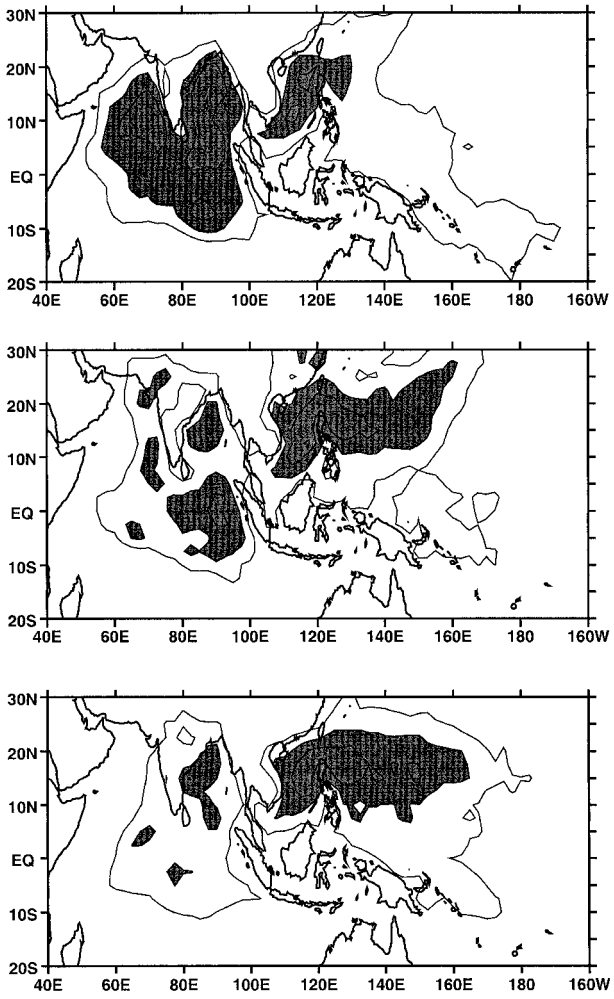

FIG. 1. Seasonal variation of 10–100-day filtered OLR variance. (top) May–Jun average, (middle) Jul average, and (bottom) Aug–Oct average. Contour interval is 250 (W m^{-2})^2. First contour at 500 (W m^{-2})^2. Regions where the OLR variance $>$ 750 (W m^{-2})^2 are shaded.

data to remove high-frequency variability. In order to examine the role of Rossby waves in the BSISO life cycle, a separate dataset containing OLR and 850-mb wind anomalies was created for which the pentad mean smoothing was not applied. (These fields appear in Figs. 6 and 7 only, and are discussed in section 4.)

The compositing strategy for this study was to select an ensemble of BSISO events and use them to form an average BSISO life cycle for early summer and another for late summer. The boreal summer was defined to be the months of May–October, and summer was further divided into the time periods May–June and August–October. Many studies (Wang and Xie 1997; Li and Wang 1994; others) have demonstrated that the mean flow and the SST distribution have a strong effect on the character of the ISO. During boreal summer, the mean climatology undergoes a shift from early to late summer. Figure 1 shows the average OLR variance for May–June, July, and August–October and displays the movement of the primary convecting region from early to late summer. During May–June, the OLR variance is concentrated in the Asian monsoon region with maxima in the Bay of Bengal, the Arabian Sea, and the eastern Indian Ocean. In August–October, the region of maximum variance shifts to the South China and Philippine Seas. July has strong variance in the Indian Ocean, as well as the South China and Philippine Seas. July is a time of transition between early and late summer and was excluded from the study.

The change in OLR variance distribution may be attributed in part to the annual cycle in SST. Figures 2a and 2c show the regions where the skin temperature—the radiative temperature of the surface—is greater than 301 K, which corresponds to the statistical criterion for deep convection (Graham and Barnett 1987). The skin temperature distribution is sufficiently different during May–June (MJ) and August–October (AO) that we may expect some difference in BSISO air–sea interactions due to the change in the atmospheric lower boundary condition. In MJ, the northern Indian Ocean, Bay of Bengal, and Arabian Sea are much warmer than in AO, as is the Indian subcontinent. The region of SSTs high enough to support deep convection extends farther into the southern Indian Ocean in MJ than in AO. In the western Pacific, the equator lies within the region of maximum temperatures in MJ; by AO, the region of highest SSTs has moved northward off the equator. This northward movement is important because the ISO has been shown to reach its maximum intensity when the thermal and geographic equators coincide (Salby and Hendon 1994).

The character of the ISO has been shown (Wang and Xie 1997) to depend upon the low-level moisture distribution, which is partly determined by the SST field. The distribution of q(1000 mb) also undergoes a shift from MJ to AO (Figs. 2b,d). In the Indian Ocean. The low-level moisture is substantially greater in the Arabian Sea, northern Bay of Bengal, and eastern Indian Ocean in MJ. In the western Pacific, q(1000 mb) is greater along the equator in MJ than in AO. Since the ISO is known to depend on frictional moisture convergence onto the equator, we may expect the difference in q(1000 mb) to cause differences in the BSISO life cycle. The vertical shear of the basic-state zonal wind is also markedly different in MJ and AO (Figs. 2a, 2c). In particular, the easterly shear is stronger in AO over the western Pacific. The difference in shear is important because vertical shear destabilizes Rossby waves (Wang and Xie 1996; Xie and Wang 1996).

Having decided upon the compositing time periods, the next step was to form the AO and MJ composites by selecting BSISO events. The events were identified by their convective signal, as measured by the OLR anomaly. Because of the different propagation modes present in the BSISO (Zhu and Wang 1993; Wang and Rui 1990), care is required in forming the composite. The ISO is generally defined to be an eastward-moving

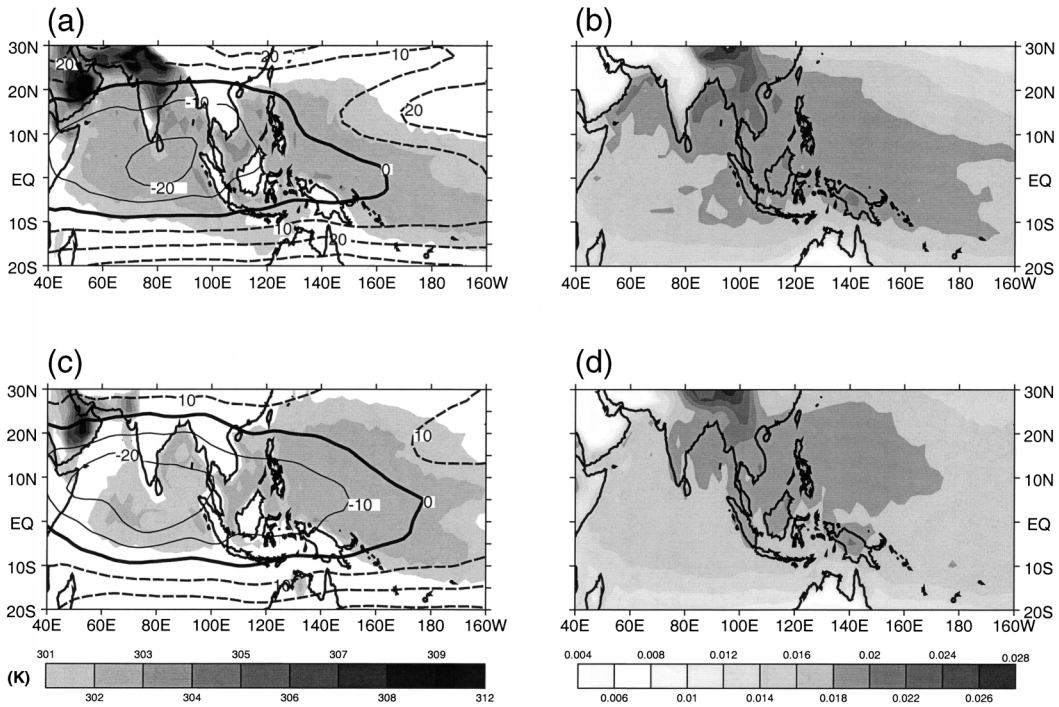

FIG. 2. Comparison of May–Jun and Aug–Oct average vertical shear of the zonal wind U(200 mb)–U(850 mb), skin temperature, and q(1000 mb). (a) May–Jun average skin temperature and vertical wind shear. Solid (dashed) contours indicate negative (positive) shear. Thick line is the zero contour. Contour interval is 10 m s^{-1}. Shading denotes skin temperature greater than 301 K [scale at bottom of (c)]. (b) May–Jun average specific humidity at 1000 mb. Shading denotes specific humidity greater than 0.004 [scale at bottom of (d)]. (c) Aug–Oct average skin temperature and vertical wind shear. Contours and shading as in (a). (d) Aug–Oct average specific humidity at 1000 mb. Shading as in (b).

envelope of convection (Madden and Julian 1994), but has westward- and northward-moving components in summer. In order to form a composite that captures the eastward-moving envelope and still retains the possibility of westward and northward movement within an ocean basin, we required a given convective event to have a large-scale signal in the Indian Ocean and subsequently (no more than 20 days later) in the western Pacific. We do not specify the direction the convection in a given ocean basin must travel, only that there be a large-scale convective envelope which is generally eastward moving. The convective signal was measured by the filtered OLR anomaly averaged over the boxed base regions in Figure 3a. If the OLR anomaly averaged over each box was < -15 W m^{-2} as the BSISO event passed overhead, the event was a possible candidate for the composite.

The Indian Ocean base region was chosen because it is within this area that equatorial BSISO convection is found most frequently (Wang and Rui 1990). The western Pacific base region was chosen because it is a region of large OLR variance and high SST for both AO and MJ (Figs. 1a,c). The evolution of the composite BSISO was not sensitive to the exact choice of the western Pacific base region, though the phase of the composite relative to the day of maximum convective intensity changes. The MJ composite is centered in time around the day on which the convective anomaly averaged over the Indian Ocean base region reaches its maximum intensity (i.e., OLR is at a minimum). The AO composite is centered around the day on which the convective anomaly averaged over the western Pacific base region reaches its maximum intensity. The basic structure of the BSISO life cycle for MJ is similar whether the composites are centered around the Indian Ocean or western Pacific base region, but the AO composite is sensitive to the choice of base region for centering the composite. While centering the AO composite around the Indian Ocean base region does not change the basic features of the composite, its statistical significance is reduced. This is because the lengths of each BSISO event were slightly different, and there was more variability in event length for AO than MJ. Centering the AO composite around the temporal center of its life cycle and its location of maximum convective intensity improved the statistical significance of the composite.

Examination of the individual events forming the composites showed that MJ events amplified in the Indian Ocean, and then moved eastward along the equator into the western Pacific and northward over the Indian subcontinent. AO events tended to show behavior similar to that of MJ in the Indian Ocean, but had two different types of behavior in the western Pacific. Most AO events showed little evidence of eastward propa-

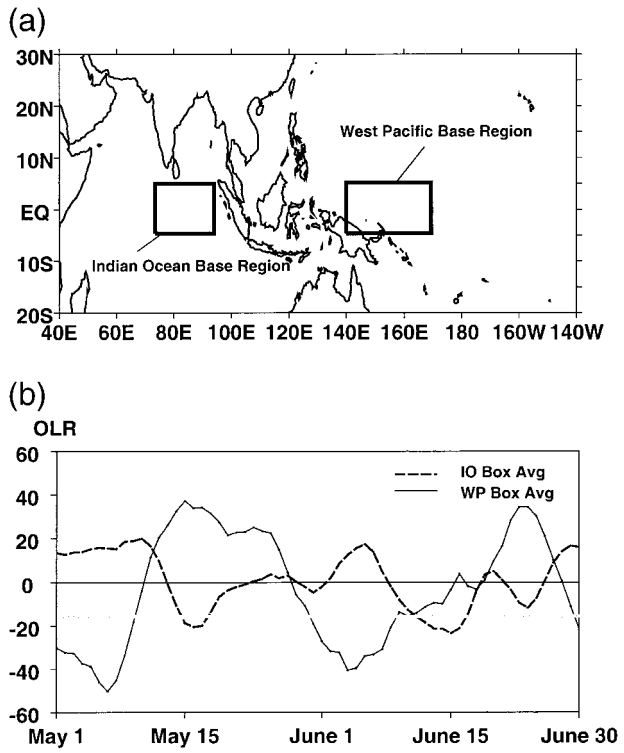

FIG. 3. Compositing procedure: (a) location of base regions used to form the composites; (b) example of event selection. OLR (W m^{-2}) anomaly time series for May–Jun 1995: Dashed line shows the OLR anomaly averaged over the Indian Ocean base region shown in (a). Solid line shows the OLR anomaly averaged over the western Pacific base region shown in (a). The gray horizontal line is located at -15 W m^{-2} and is the intensity threshold an event must reach to be included in the composite.

gation along the equator, and were marked instead by northwestward propagation from the equator to the South China Sea, and subsequent westward propagation toward the Bay of Bengal. Out of 18 events, however, 5 showed structure much like that of the eastward-propagating MJ events. Averaging the two types of AO events together tends to skew the composite toward the eastward-propagating events because they have greater amplitude. However, it was found that of five eastward-propagating AO events, four occurred within five days of the start or end of the AO compositing period. The five eastward-propagating events were eliminated from the composites, and we retained only the northwestward-propagating mode, which seems to be more characteristic of AO.

Figure 3b illustrates the event selection procedure for MJ for the year 1995. The OLR averaged over the base region in Fig. 3a shows two candidate events occurring during the period May–June for which the Indian Ocean and west Pacific base region averaged OLR minima were less than -15 W m^{-2} and out of phase with one another. Therefore, for 1995, the events to be included in the MJ composite had their OLR minima on 7 May and 3 June. The compositing procedure described above produces an ensemble of 22 events for May–June and 13 for August–October. Though the AO time period is longer than that of MJ, there are fewer events composing the AO composite than the MJ composite. This is because the BSISO has greater interannual variability in AO than in MJ, with some years having no events in AO and some having as many as three. For MJ, there were no years in which the BSISO was absent.

The statistical significance of the composited fields was assessed using the Student's *t* test, after first applying the *f* test to determine that the use of the *t* test was appropriate (Press et al. 1986). The null hypothesis used to test the significance of the composites was that there are no coherent anomalies in the 10–100-day band during boreal summer. To test this hypothesis, a synthetic composite was constructed using an ensemble of events whose members had the value zero. This synthetic composite had the same number of members as the real composites; that is, 22 for May–June and 13 for August–October, giving the *t* test 42 degrees of freedom for May–June and 24 degrees of freedom for August–October.

3. The BSISO life cycle in May–June and August–October

We will use spatial anomaly maps of the BSISO to examine its life cycle in terms of OLR and low-level winds. Figures 4 and 5 show the OLR and 850-mb wind vector anomalies for MJ and AO. From day -10 to day -5, initiation of convection in the Indian Ocean occurs in both composites, and, on day 0, convective anomalies in the Indian Ocean region reach their maximum intensity. The transition of convection from the Indian Ocean to the western Pacific occurs during the period from day $+5$ to day $+15$, and dissipation of the current BSISO cycle and initiation of the next takes place during day $+20$ to day $+30$. We will briefly describe each phase and then discuss differences between MJ and AO for that phase. For the purpose of comparing the two life cycles, day 0 for each composite was defined to be the day on which maximum convective intensity in the Indian Ocean base region occurred. The MJ composite was centered about the day on which OLR was a minimum over the Indian Ocean base region, so that day 0 is the day on which convection in MJ reaches maximum intensity. However, the AO composite is centered about the day on which OLR was a minimum over the west Pacific base region, so the AO composite reaches maximum intensity on day $+15$.

a. Initiation: Day −10 to day −5

The initiation of the BSISO cycle in both MJ and AO is marked by the appearance of convection (Figs. 4a and 5a) in the equatorial Indian Ocean and subsequent eastward and poleward propagation. During the initiation of convection in the Indian Ocean, there is anticyclonic

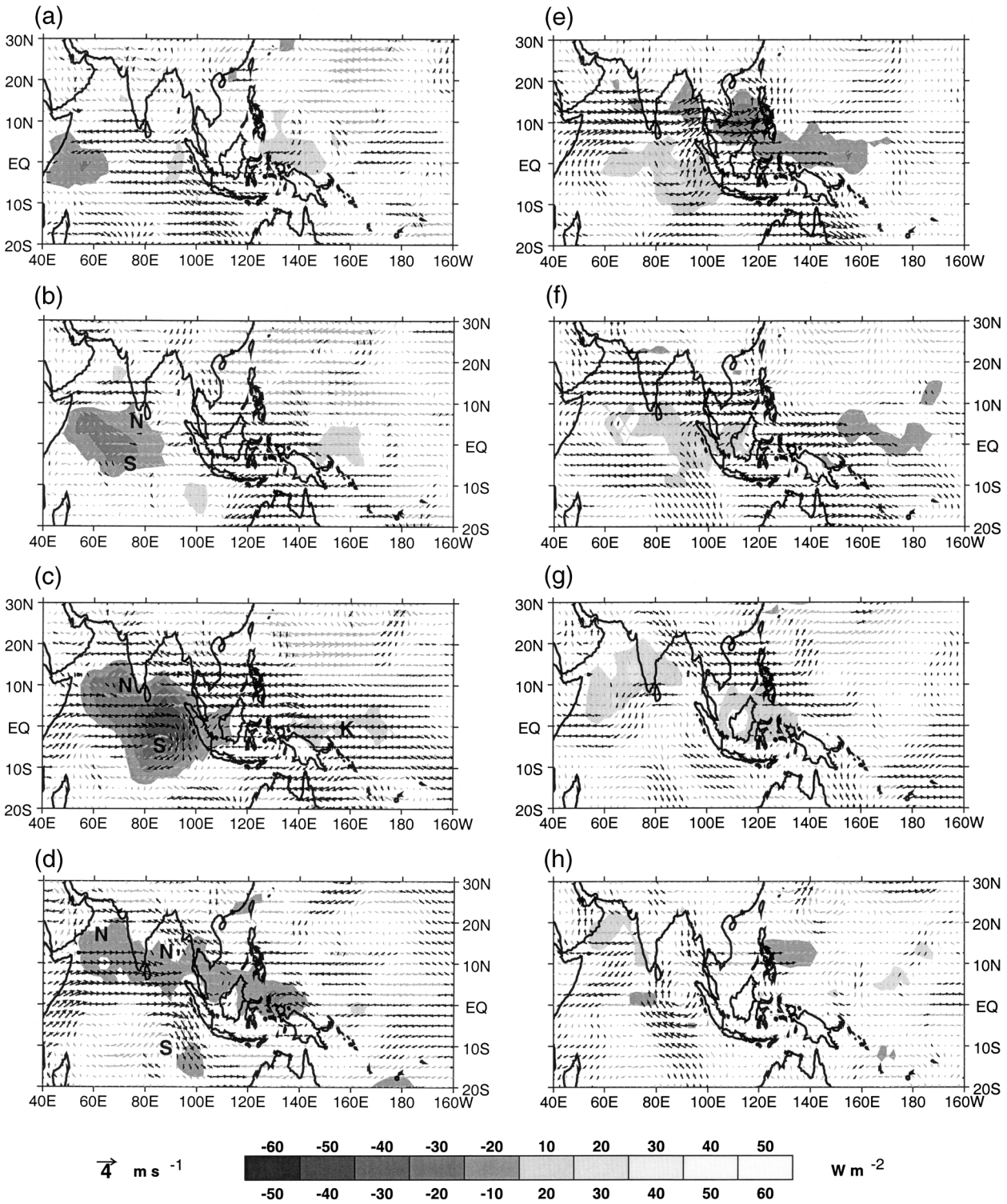

FIG. 4. May–Jun composite OLR and 850-mb wind anomalies. Contours are OLR (W m^{-2}). Gray arrows are 850-mb wind vector anomaly. Black arrows are 850-mb wind anomaly significant at the 90% confidence level. Shown are (a) day −10, (b) day −5, (c) day 0, (d) day +5, (e) day +10, (f) day +15, (g) day +20, and (h) day +25. The numbers above and below the gray shades at the bottom of the figure indicate the range of values represented by that gray shade.

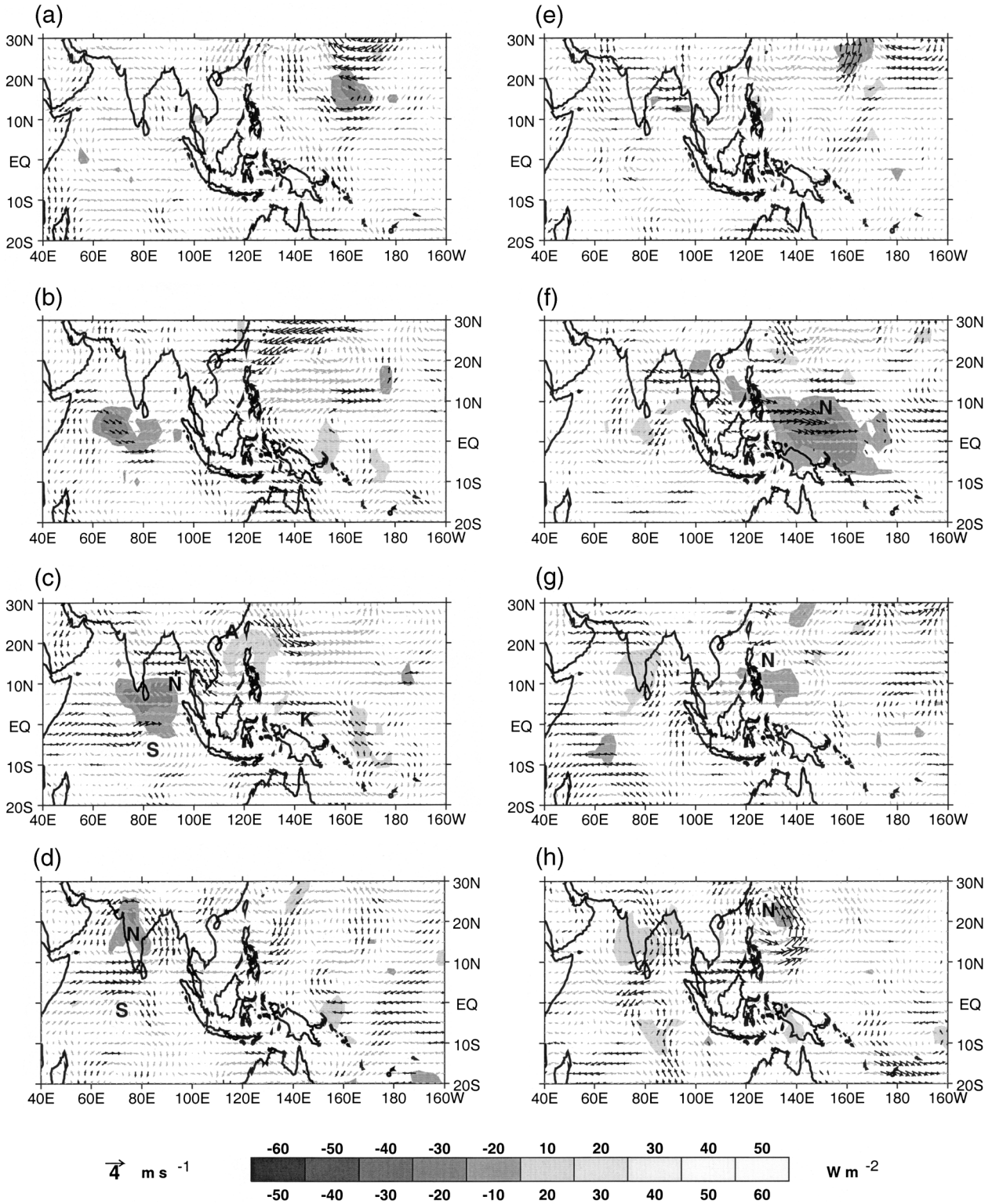

FIG. 5. Aug–Oct composite OLR and 850-mb wind anomalies. Contours and wind vectors are as in Fig. 4. Shown are (a) day −10, (b) day −5, (c) day 0, (d) day +5, (e) day +10, (f) day +15, (g) day +20, and (h) day +25. The numbers above and below the gray shades at the bottom of the figure indicate the range of values represented by that gray shade.

flow at 850 mb over the Bay of Bengal, Arabian Sea, and the Indian subcontinent in both MJ and AO. These anticyclones are associated with low-level outflow from large-scale subsidence (not shown). The northern Indian Ocean is occupied predominantly by 850-mb easterlies. These easterlies move northward ahead of the convection, and westerlies appear within and behind the convection by day −5. On day −5, both AO and MJ show a region of suppressed convection in the equatorial western Pacific.

Though the onset of the BSISO cycle is similar in MJ and AO, there are several important differences. The MJ convective anomaly forms over Africa and the western equatorial Indian Ocean, growing into a well-organized anomaly centered at 55°E by day −10 (Fig. 4a). This is marked contrast to the AO case, in which the convective anomaly amplifies in the central Indian Ocean east of 60°E and does not become well organized until day −5 (Fig. 5b). This is because, in the AO case, the monsoon gyre has had time to spin up and to cause upwelling along the coast of Africa [Webster et al. (1998) and Fig. 2b]. This cooler water inhibits the formation of deep convection in the western equatorial Indian Ocean. In the MJ case, the sea surface along the African coast has not yet cooled (Fig. 2a). Convection in MJ during day −10 to day −5 is centered on the equator, while the AO convective anomaly lies almost entirely within the Northern Hemisphere. This is consistent with the greater equatorial asymmetry in SSTs and low-level moisture in AO, with higher values to the north of the equator favoring convection there. Because MJ is centered along the equator, frictional moisture convergence may help to amplify the anomaly and increase its amplitude beyond that of AO.

b. Peak phase: Day 0

Convection in both MJ and AO reaches peak intensity in the Indian Ocean on day 0. The region of maximum convection has moved to the equatorial eastern Indian Ocean and the convective anomalies elongate to the north and south, as Rossby waves are emitted. This will be discussed further in section 4. The 850-mb flow on day 0 is characterized by a strong cyclonic circulation centered near the southern tip of India for MJ and in the southern Bay of Bengal for AO (marked N in Figs. 4c and 5c). Easterlies lie north of the convection and westerlies are found within and to the south of the convective anomaly. Corresponding cyclones are found in the Southern Hemisphere (marked S in Figs. 4c and 5c) and are the result of Rossby wave emission. In both MJ and AO, a Kelvin wave response (marked K in Figs. 4c and 5c) extends well into the equatorial western Pacific.

The MJ convective anomaly is more intense that that of AO, and extends farther into the southern Indian Ocean, Arabian Sea, and Bay of Bengal. This is due to the greater SSTs and low-level moisture in MJ in these regions (Fig. 2). Another difference between MJ and AO is the character of the flow over the Maritime Continent and the South China Sea. In MJ, a region of strong 850-mb easterlies is located over the Maritime Continent in MJ. In AO, the band of easterlies to the northeast of the convection is weaker, and there is an anticyclone over the South China Sea collocated with the region of suppressed convection there. The strong easterlies in MJ cause strong convergence and latent heat flux anomalies (not shown) to the east of the convection, and are conducive to its eastward movement. The corresponding AO anomalies are much weaker.

The patterns of suppressed convection in the western Pacific are different on day 0, with the maximum suppression in AO occurring north of the Philippines while that of MJ lies along the equator. This is a result of very different evolution of the suppressed anomaly between day −5 and day 0. The MJ suppressed anomaly remains on the equator, while in AO the equatorial suppressed anomaly emits a Rossby wave that travels northward, reaching the South China Sea by day −5. (This will be discussed further in section 5.) This difference in the patterns of suppression affects air–sea interactions and the character of subsequent convection in the western Pacific.

c. Transition of convection from the Indian Ocean to the western Pacific: Day +5 to day +10

During the period from day +5 to day +10, convection moves northward and weakens over the Indian subcontinent in both MJ and AO. The Indian Ocean is dominated by two circulation patterns: a cyclone associated with the convection and a second cyclone south of the equator (marked N and S in Figs. 4d and 5d). Strong westerly wind anomalies lie between these two circulation centers. By day +5, the equatorial Kelvin wave response in both MJ and AO is damped as the convection in the Indian Ocean moves northward off the equator. Convection in the equatorial Indian Ocean becomes suppressed.

At this point, the MJ and AO BSISO life cycles diverge dramatically. In MJ, convection moves eastward across the Maritime Continent and into the equatorial western Pacific. In AO, however, no such eastward propagation occurs. Convective anomalies do not cross the Maritime Continent; instead, convection in the western Pacific appears along the equator and organizes between day +10 and day +15. The MJ and AO 850-mb wind anomalies evolve differently as well. In MJ, there is a cyclone associated with convection over the South China Sea, while in AO, the South China Sea is a region of anticyclonic flow and suppressed convection. In the equatorial western Pacific, there are westerlies within the convection in MJ, and no corresponding feature in AO, in which convection is only beginning to organize along the equator.

d. Dissipation of current BSISO cycle and initiation of the next cycle: Day +15 to day +30

In MJ and AO at day +15, convection in the eastern and central equatorial Indian Ocean is suppressed (Figs. 4f and 5f). There is an anticyclone at 850 mb coincident with the region of suppressed convection. A band of westerly winds oriented northwest–southeast extends from India to the western Pacific.

In MJ, there is convection along the equator in the western Pacific that has propagated eastward since day +10. Between day +15 and day +20, the convection along the equator dissipates. The panel for day +25 shows a small area of northwestward-moving convection similar to that in AO. By day +30 (not shown), the composite has wrapped around to the next BSISO cycle, giving a period of about 40 days.

In AO, a strong convective anomaly appears in the western Pacific on day +15. Between day +15 and day +30 (not shown), convection moves northwestward, dissipating by day +35 (not shown). This convection has the form of a highly asymmetric Rossby wave emitted by the convection that forms along the equator during day +10 to day +15. (See section 4 for further discussion.) The northward-moving convective anomaly is accompanied by a cyclonic circulation oriented so that easterlies lie to the north of the convection, and westerlies within it and to its south. The southward-moving anomaly dissipates. Between day +30 and day +35 (not shown), the AO composite wraps around, giving a period similar to that of MJ. The life cycle shown here is similar in many ways to those found in two recent studies of the intraseasonal variability of the Asian monsoon.

Annamalai and Slingo (2000, manuscript submitted to *Climate Dyn.*, hereinafter ANSL) examined the active and break cycles of the Asian monsoon, and found the intraseasonal variability to be concentrated in a 40-day mode and a 15-day mode. They used principal oscillation pattern analysis to look at the evolution of the two modes. The life cycle of their 40-day mode (which they find to be strongest in the onset phase of the monsoon) is similar to the MJ life cycle, showing pronounced eastward propagation along the equator and northward propagation in the Indian Ocean. They also observe northward propagation of convection and circulation anomalies in the western Pacific, as in the AO composite, and they identify this northward movement with Rossby waves. In addition they note the presence of Rossby waves associated with convection in the Indian Ocean.

Lawrence and Webster (2000, manuscript submitted to *J. Climate*, hereinafter LW) also composited the BSISO over the entire summer using EOF analysis. They filtered to eastward-moving wavenumbers 1–3 and saw a structure similar to the MJ composite in the Indian Ocean, with Rossby waves emitted to the north and south of the equatorial convection. They explain the northward propagation of convection in the Indian Ocean as convergence into the northern lobe of the Rossby wave. In the western Pacific, their composite is similar to our MJ mode, and does not show northwestward propagation of convection. This may be a result of filtering so that only eastward-moving waves were retained.

4. Rossby waves

A key result of Wang and Xie (1997) was that Rossby waves play a critical role in the BSISO. Since the life cycle discussed in section 3 shows an evolution similar to the modeled life cycle of Wang and Xie, including evidence of Rossby waves, we constructed a separate dataset of OLR and 850-mb winds to examine these westward-moving waves more closely. Because Rossby waves have a relatively high wavenumber spatial and temporal scale, we use data filtered as described in section 2, except that the running pentad mean smoother is not applied. This gives a 1–100-day bandwidth, which allows us to look at the structure of Rossby waves in more detail than in section 3.

a. Rossby wave emanation from equatorial Indian Ocean convection in MJ

In this section, we will describe Rossby wave emanation from equatorial convection in MJ in the Indian Ocean. Rossby wave emission in AO is similar to MJ in structure and phase, but weaker in amplitude, so we limit our discussion to MJ for the sake of brevity. Between day −7 and day −3 in MJ (Figs. 6a and 6b), convection moves eastward along the equator, intensifying and extending farther to the north and south. By day −3, the convection grows stronger, and the wind structure at 850 mb consists of anomalous easterlies to the east of the convection, and westerlies within and to the west of the convection. To the north and the south are circulation structures (marked N1 and S1 in Fig. 6b), which project strongly onto the Rossby wave response to equatorial convection predicted by Matsuno (1966) and Gill (1980). By day +1, the region of maximum convective intensity has reached the west coast of Sumatra, and the wind anomaly structure has become asymmetric about the equator. The Rossby lobe marked N1 has moved northwestward. In the Southern Hemisphere the Rossby lobe S1 has also moved to the west. Meanwhile, two new lobes (marked N2 and S2 in Fig. 6c) have appeared. Between day +1 and day +4, these circulation centers move poleward and westward. Convection and circulation anomalies associated with the northern Rossby cells are larger and more intense than those of the southern cells. The convection associated with the southern lobe S1 dies away upon moving over the colder water of the southern Indian Ocean. Between day +5 and day +6, convection becomes suppressed along the equatorial Indian Ocean and enhanced over

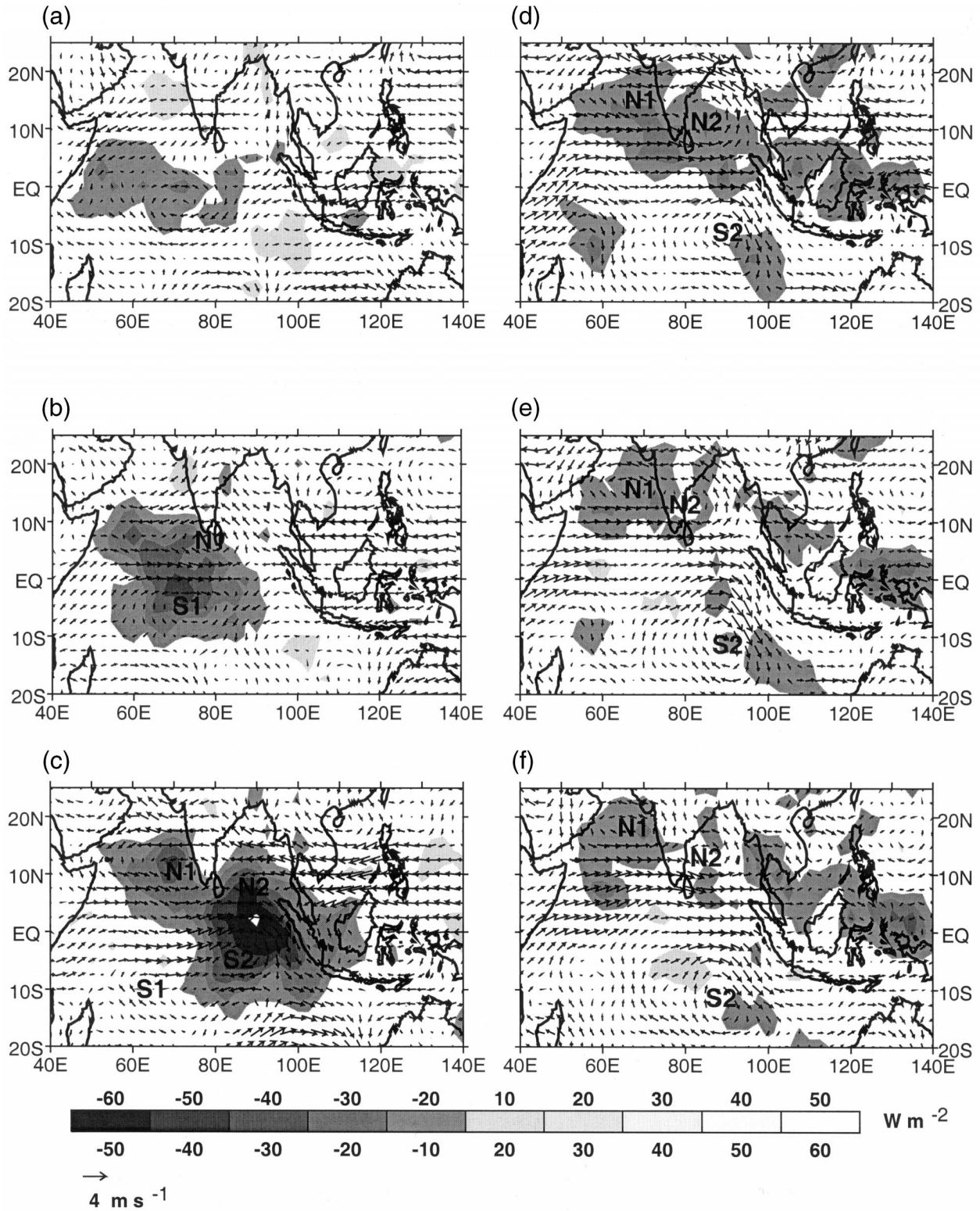

FIG. 6. May–Jun 1–100-day filtered 850-mb wind and OLR anomalies. Contours are OLR anomaly, with first contour at 10 W m^{-2}. Vectors are the 850-mb wind anomaly. Shown are (a) day −7, (b) day −3, (c) day +1, (d) day +4, (e) day +5, and (f) day +6. The numbers above and below the gray shades at the bottom of the figure indicate the range of values represented by that gray shade.

the Maritime Continent and the equatorial western Pacific. Meanwhile, the convection and associated cyclonic wind anomalies N1 and N2 begin to weaken.

Rossby wave emanation in MJ is highly asymmetric. In the absence of vertical wind shear, the Rossby wave with the gravest meridional index is characterized by a pair of low-level cyclones symmetric about the equator (Matsuno 1966; Gill 1980). Easterly vertical shear can substantially distort the structure of equatorial Rossby waves (Xie and Wang 1996; Wang and Xie 1996). Easterly shear favors enhancement of equatorial Rossby waves and tends to confine the Rossby wave to the lower troposphere so that the low-level cyclone is stronger than the corresponding upper-level anticyclone (Wang and Xie 1996).

The Rossby wave evolution in the Indian Ocean in MJ is similar to that in the model results of Wang and Xie (1997). In this model, the eastward-moving equatorial disturbance in the Indian generates poleward-propagating Rossby waves. These waves behave much like those in the MJ composite in the Indian Ocean, with the northern lobe greater in amplitude than the southern lobe. Wang and Xie attributed the selective amplification of the northern lobe to the mean vertical shear of the monsoon flow and the basic-state low-level humidity. The easterly shear north of about 10°S destabilizes the northward-moving Rossby waves, while south of 10°N, the shear is westerly (Fig. 2a) and does not amplify the southward-moving waves. The centers of convergence associated with the northern Rossby lobes move over a region of warmer SSTs and higher q(1000 mb) than do those of the southern lobe (Figs. 2a, 2b); therefore, the northern lobe is reinforced, while the southern lobe decays.

Rossby wave emanation from the equatorial Indian Ocean was also noted by LW and ANSL. Krishnan et al. (2000) saw Rossby wave propagation of the suppressed convective anomalies prior to monsoon break periods. The behavior of the northward-propagating suppressed anomalies is similar to that of the enhanced anomalies seen in MJ and AO (not shown).

b. *Emanation from equatorial convection in the western Pacific in AO*

As discussed in section 3, one of the most significant differences between MJ and AO is that westward-moving convection and circulation anomalies in the western Pacific are strong in AO and much less pronounced in MJ. In this section, we will look at Rossby wave emission in AO in the western Pacific.

In AO, on day +9 (Fig. 7a), convection is beginning to organize in the equatorial western Pacific, and by day +11, a meridionally confined band of convection appears just south of the equator. Two cyclonic circulation anomalies lie north of the convection. By day +13, the convective anomaly has intensified and moved westward and poleward. The cyclonic pattern (marked N in Fig. 7c) has consolidated and strengthened, and westerlies appear within the convection. As the most intense region of the convection moves northward off the equator, a southern lobe of convection appears along with an associated cyclonic wind anomaly marked S in Fig. 7c. As in MJ in the Indian Ocean, the ambient shear and the distribution of low-level moisture favor the northern lobe, which is much stronger and moves away to the north while the southern lobe is reduced in strength by day +19. The evolution of convection and the low-level wind anomalies in AO during day +11 to day +19 is similar to that of MJ in the Indian Ocean during day −7 to day +6. In both cases, equatorial convection emits Rossby waves to the north and the south, with the northern lobe amplified more than the southern lobe. The selective amplification of the northern Rossby cell is likely due to the mean state, with regions of maximum SST, low-level moisture, and easterly vertical wind shear all lying north of the equator.

The northwestward propagation of convection in AO is similar to the Rossby wave emanation from equatorial convection in the western Pacific illustrated in Wang and Xie (1997), though the pattern here is shifted west relative to the model results. As in Wang and Xie, we see enhancement of the Rossby wave mode in AO, and weakening of the equatorial Kelvin mode in accordance with the increased vertical shear relative to MJ. Northwestward-moving Rossby waves with ~10 day period were documented in detail by Lau and Lau (1990) and more recently by ANSL. This 10-day mode is similar in structure to the waves found in the AO composite, though the relationship between the 10-day mode and the BSISO is not clear.

5. Air–sea interaction in the BSISO

a. *Air–sea interaction in the northward–propagating mode in MJ*

In this section, we will present evidence that air–sea interaction accompanies the northward propagation of convection anomalies in the Indian Ocean. (For the sake of brevity, only MJ will be described; AO is similar in evolution, though weaker in amplitude.) Figure 8 shows Hovmoeller diagrams depicting phase relationships among several fields expected to show the signature of air–sea interaction (Hendon and Glick 1997; Woolnaugh et al. 2000; etc.).

Figure 8a shows the suppressed and enhanced OLR and ω(500 mb) anomalies. The OLR indicates convection beginning in the vicinity of the equator on day −7. There is subsequent intensification along the equator and poleward propagation, with the northward-propagating branch much stronger and longer lived than the southward-propagating branch. The northward and southward-propagating convective signals are consistent with Figs. 8d and 4a and reflect the emission of Rossby waves from equatorial convection. The suppressed OLR and

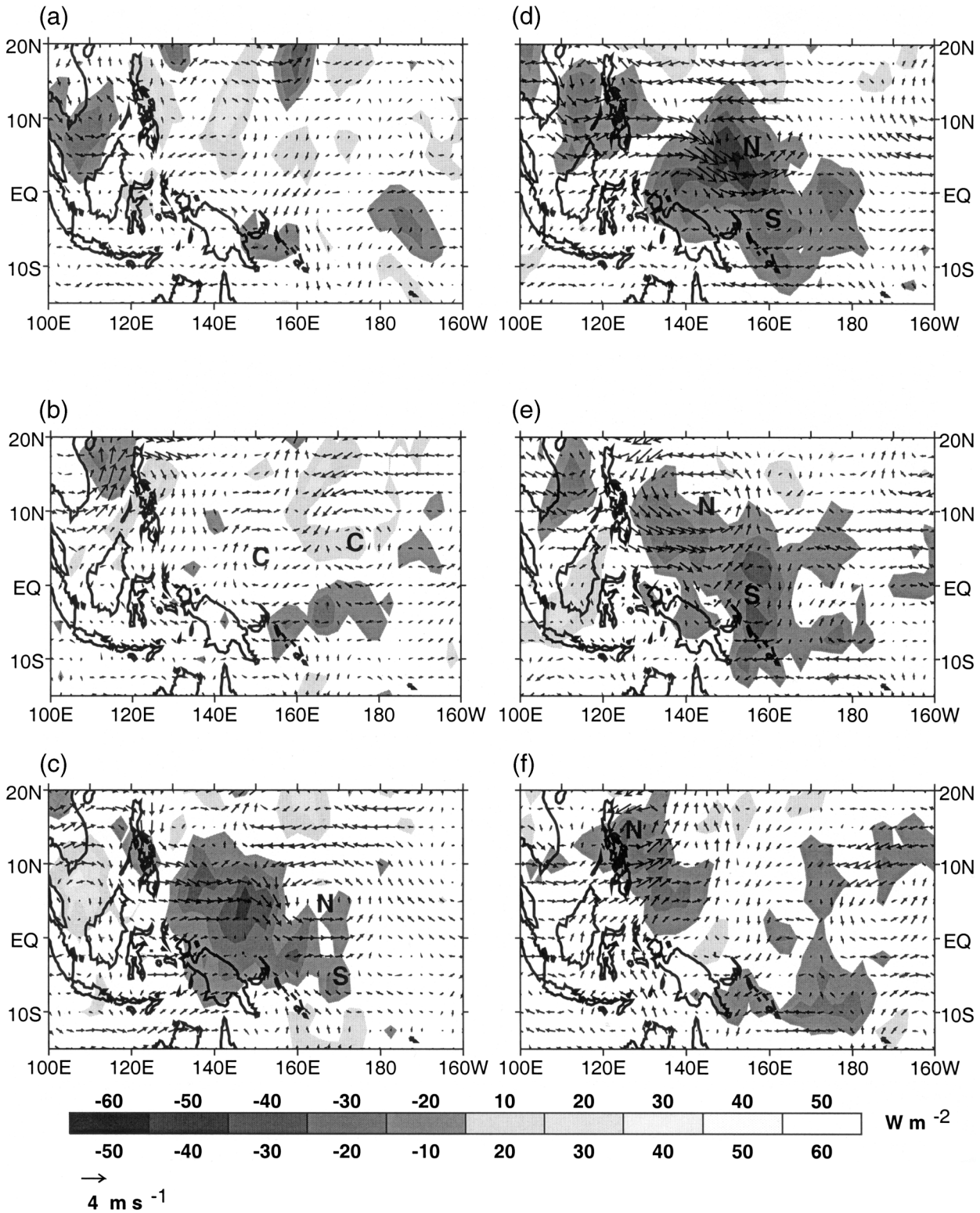

FIG. 7. Aug–Oct 1–100-day filtered 850-mb wind and OLR anomalies. Contours as in Fig. 6. Shown are (a) day +9, (b) day +11, (c) day +13, (d) day +15, (e) day +17, and (f) day +19. The numbers above and below the gray shades at the bottom of the figure indicate the range of values represented by that gray shade.

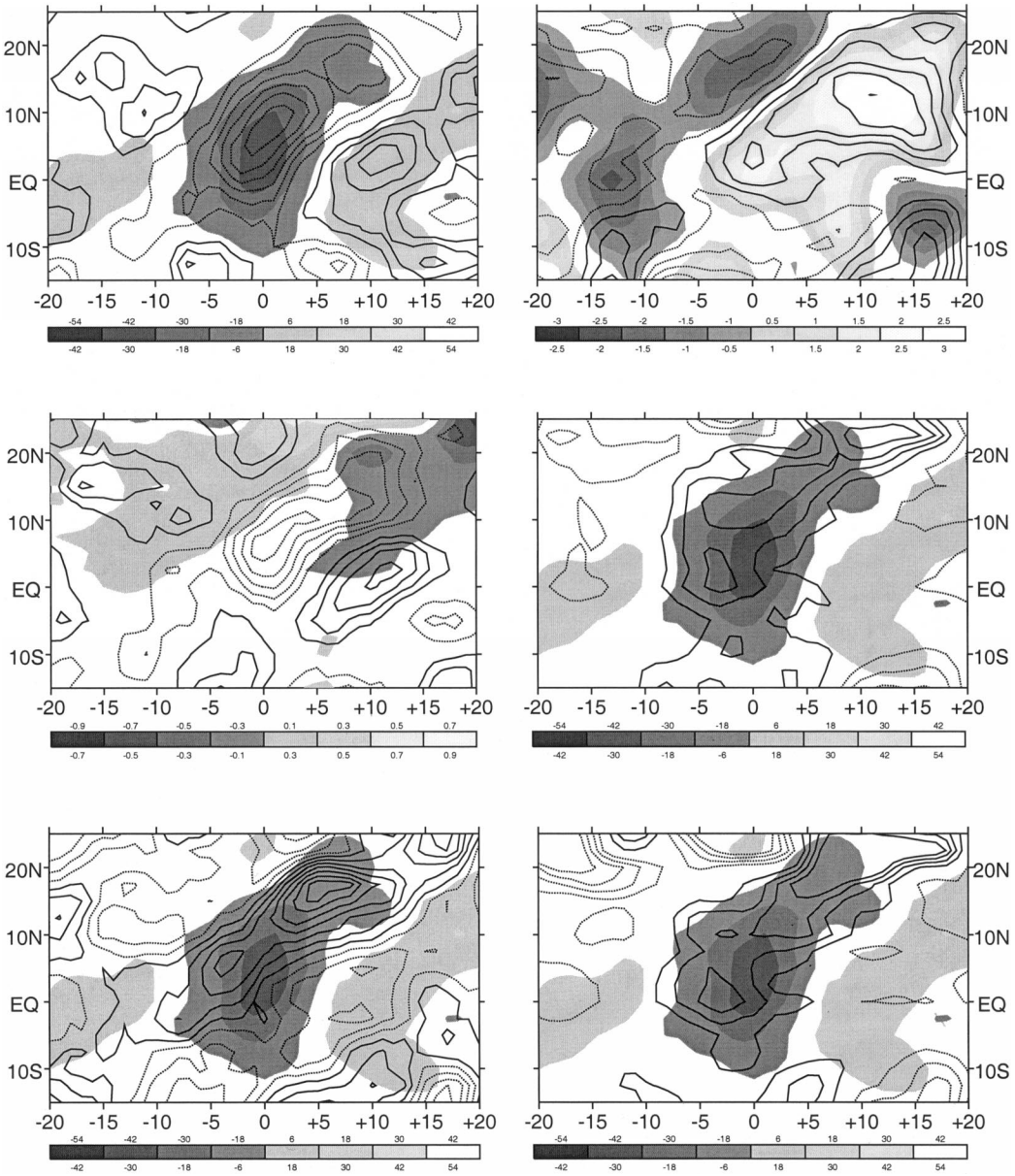

FIG. 8. May–Jun Hovmoeller diagram for 65°–95°E. The abscissa is time in days relative to day 0 of the composite. The numbers above and below the gray shades at the bottom of the figure indicate the range of values represented by that gray shade. Shown are (a) the ω(500 mb) and OLR, (b) skin temperature and DSWRF, (c) OLR and convergence (10 m), (d) 850-mb zonal wind and latent heat flux, (e) moist static energy h at 1000 mb and OLR, (f) OLR and Lq(1000 mb). Scales are as follows: (a) shaded contours are OLR, dashed (solid) lines indicate upward (downward) motion at 500 mb, contour interval is 0.004 Pa s^{-1}, and first contour is at 0.004 Pa s^{-1}. (b) Shaded contours are skin temperature, solid (dashed) contours indicate positive (negative) DSWRF anomaly, contour interval is 3 W m^{-2}, and the first contour is at 3 W m^{-2}. (c) Shaded contours are OLR, solid (dashed) lines indicate positive (negative, i.e., divergence) convergence anomaly, and contour interval is 2×10^{-7} s^{-1}. First contour is at 1×10^{-7} s^{-1}. (d) Shaded contours are U(850 mb), solid lines indicate positive (negative) latent heat flux anomaly, contour interval is 6 W m^{-2}, and the first contour is at 3 W m^{-2}. (e) Shaded contours are OLR. Solid (dashed) lines indicate positive (negative) h anomaly. First contour is 300 J kg^{-1}, and the contour interval is 300 J kg^{-1}. (f) Shaded contours are OLR, and Lq(1000 mb) is scaled in the same manner as h (1000 mb) in (e).

ω(500 mb) anomalies propagate poleward, as documented by Krishnan et al. (2000) for the break phase of the Asian monsoon. The OLR and ω(500 mb) anomalies are in phase, with upward (downward) motion at 500 mb coinciding with enhanced (suppressed) convection. In regions of subsidence, a positive downward shortwave radiation flux (DSWRF) anomaly forms as a result of the reduction in cloud cover (Fig. 8b). During

day −20 to day −15, a positive skin temperature anomaly forms between the equator and 10°N and moves northward (Fig. 8b). After the positive skin temperature anomaly forms near the equator, low-level convergence appears there around day −15, and equatorial convection begins by day −7. Convection increases the cloud cover, so that the northward-moving convection is accompanied by a negative DSWRF anomaly (Fig. 8b). In the wake of the negative DSWRF anomaly, a northward-propagating negative skin temperature anomaly appears.

The 10-m convergence anomaly propagates northward along with the convective anomaly (Fig. 8c). The convergence is the results of strong easterlies to the north of the convection and westerlies within and to the west of it (Fig. 8d). The relative phase of convergence and convection changes with latitude. Convergence leads convection at the equator, consistent with the MJO results of Maloney and Hartmann (1998) and Hendon and Salby (1994), and is either in phase with the negative OLR anomaly or lagging it slightly north of about 7°N.

During the phase of the BSISO when convection is suppressed over the Indian Ocean, 850-mb easterlies are found there (Figs. 8d and 4a). The arrival of these easterlies coincides with the development of a negative latent heat flux anomaly, indicating that moisture is being transferred out of the ocean and into the atmosphere. As the easterly anomalies move to the north, the negative latent heat flux anomaly moves along in phase. With the formation of the negative latent heat flux anomaly, the negative Lq(1000 mb) (L and q are defined below) anomaly erodes (Fig. 8f) and is replaced by a positive anomaly about the same time that the 10-m convergence anomaly becomes positive and convection begins. Along the equator, the 10-m convergence and the negative latent heat flux anomaly are in phase, but north of 5°N, the negative latent heat flux anomaly leads the positive convergence anomaly. The formation of the latent heat flux anomaly approximately 10 days before the positive convergence anomaly suggests that the latent heat flux and, hence, air–sea interaction, play a role in conditioning the atmosphere for BSISO convection, particularly in the off-equatorial regions. The latent heat flux anomaly acts to remove the widespread negative q(1000 mb) anomaly in the Indian Ocean and to build up the low-level moisture, priming the atmosphere for the arrival of the positive low-level convergence anomaly.

Figure 8e shows how instability develops along the leading edge of the convective anomaly, causing the convection to propagate northward. The buildup of low-level moisture and moist static energy has been shown in other studies (Maloney and Hartmann 1998; Kemball-Cook and Weare 2001) to precede convection in the MJO. The moist static energy h is given by $h = C_pT + Lq + gz$, where C_p is the specific heat of air at constant pressure, T is air temperature, L is the latent heat of condensation, q is the specific humidity, and z is the geopotential height. Here, the 1000-mb moist static energy anomaly leads the convective anomaly at the equator and to the north of it. Examination of the terms composing h shows a positive Lq anomaly (Fig. 8f), which coincides well with the positive h anomaly, suggesting that h is largely controlled by the moisture term. A positive C_pT anomaly (not shown) leads the positive anomalies of h and Lq to the north but is too small too be seen on the same scale as Lq. The results shown above are consistent with those of LW, who noted a similar pattern of SST anomalies associated with BSISO convection in the Indian Ocean.

b. Air–sea interaction in the westward-propagating mode in AO and MJ

In the following section, we describe the role of air–sea interaction in the northwestward propagation of convection in the western Pacific in the latter half of the BSISO cycle. Differences between the MJ and AO cases will be discussed. Figures 9 and 10 show Hovmoeller diagrams of quantities relevant to air–sea interaction for AO and MJ in the western Pacific.

The pattern of air–sea interaction for AO in Fig. 9 is similar to that in MJ and AO in the Indian Ocean. On day −5, convection is suppressed in the equatorial region, and there is downward motion at 500 mb. Rossby waves emanate poleward from this region of suppressed convection, with the northern lobe more intense and propagating farther poleward than the southern lobe. In the region of downward motion preceding the convection, a positive DSWRF anomaly forms, followed by a positive skin temperature anomaly (Fig. 9b). As the positive skin temperature anomaly forms along the equator, a positive convergence anomaly develops (Fig. 9c). The convergence anomaly increases the low-level moisture, generating positive Lq(1000 mb) and h(1000 mb) anomalies (Figs. 9f,e). This makes the atmosphere unstable and leads to convection along the equator by day +11.

Equatorial convection in AO reaches a maximum on the equator on day +15 and then emanates Rossby waves to the north and south (Fig. 9a). The northern Rossby lobe propagates northwest, while the weaker southern lobe dies away by day +20. The northward-propagating positive skin temperature and DSWRF anomalies and negative latent heat flux anomaly lead the convection northward. The positive anomalies of Lq(1000 mb) and h(1000 mb) also track northward just ahead of the convection.

In MJ, on the other hand, convection moves into the western Pacific from the north and west, as shown in Figure 4. This is in marked contrast to AO, in which convection appears in the Pacific without first propagating across the Maritime Continent. In MJ, the suppressed region lies mostly along the equator (Figs. 4b, 4c, and 10a). Like the convective anomaly, the suppressed anomaly arrives from the northwest. Rossby

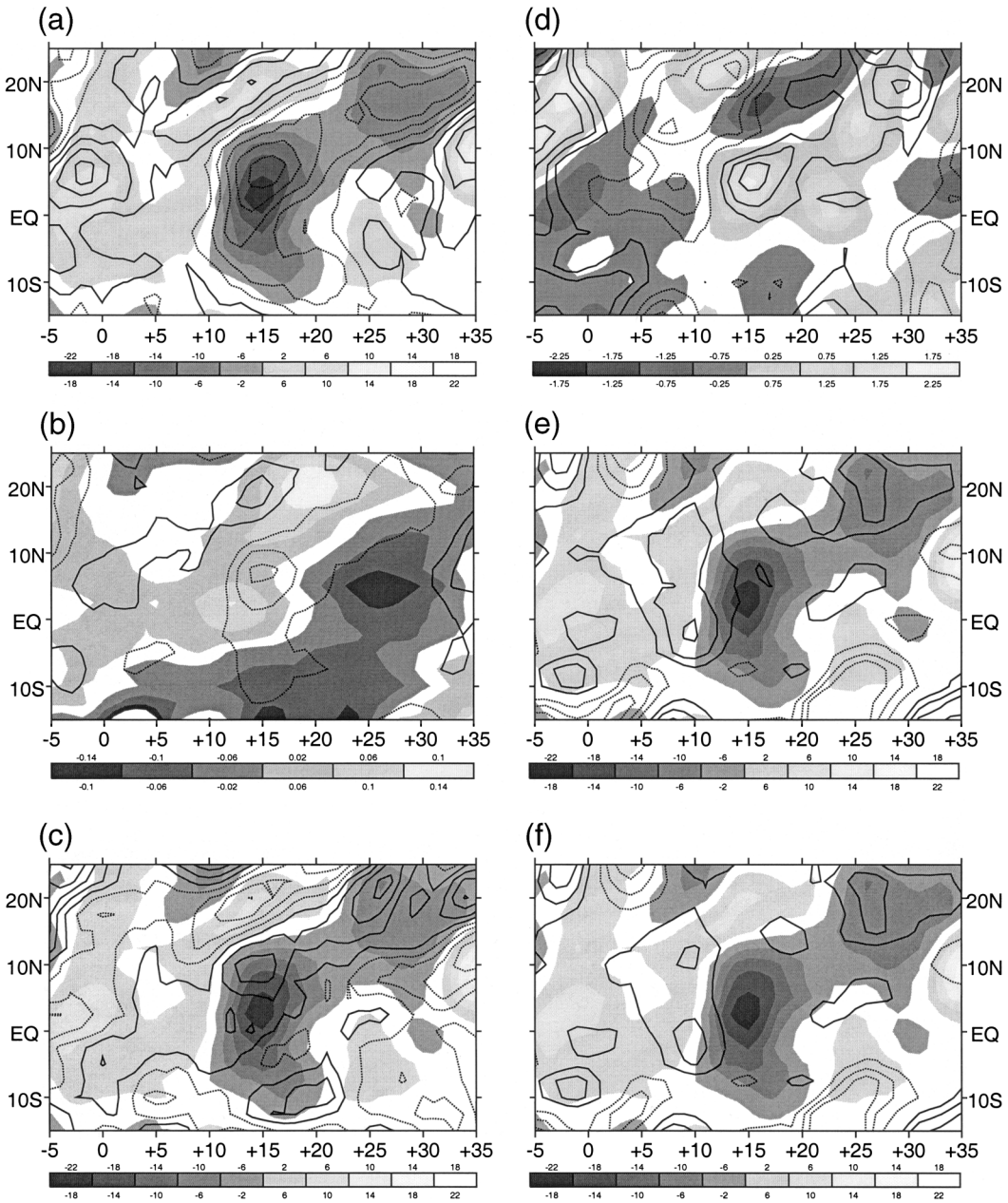

FIG. 9. Aug–Oct Hovmoeller diagram for 125°–170°E. The abscissa is time in days relative to day 0 of the composite. The numbers above and below the gray shades at the bottom of the figure indicate the range of values represented by that gray shade. Shown are (a) the ω(500 mb) and OLR, (b) skin temperature and DSWRF, (c) OLR and convergence (10 m), (d) 850-mb zonal wind and latent heat flux, (e) moist static energy at 1000 mb and OLR, (f) OLR and Lq(1000 mb). Scales are as follows: (a) Shaded contours are OLR, dashed (solid) lines indicate upward (downward) motion at 500 mb, contour interval is 0.004 Pa s^{-1}, and first contour is at 0,002 Pa s^{-1}. (b) Shaded contours are skin temperature, solid (dashed) contours indicate positive (negative) DSWRF anomaly, contour interval is 4 W m^{-2}, and the first contour is at 4 W m^{-2}. (c) Shaded contours are OLR, solid (dashed) lines indicate positive (negative, i.e., divergence) convergence anomaly, contour interval is 2×10^{-7} s^{-1}, and first contour is at 1×10^{-7} s^{-1}. (d) Shaded contours are U(850 mb), solid lines indicate positive (negative) latent heat flux anomaly, contour interval is 4 W m^{-2}, and the first contour is at 4 W m^{-2}. (e) Shaded contours are OLR. Solid (dashed) lines indicate positive (negative) h anomaly. First contour is 200 J kg^{-1}, and the contour interval is 200 J kg^{-1}. (f) Shaded contours are OLR, and Lq(1000 mb) is scaled in the same manner as h(1000 mb) in (e).

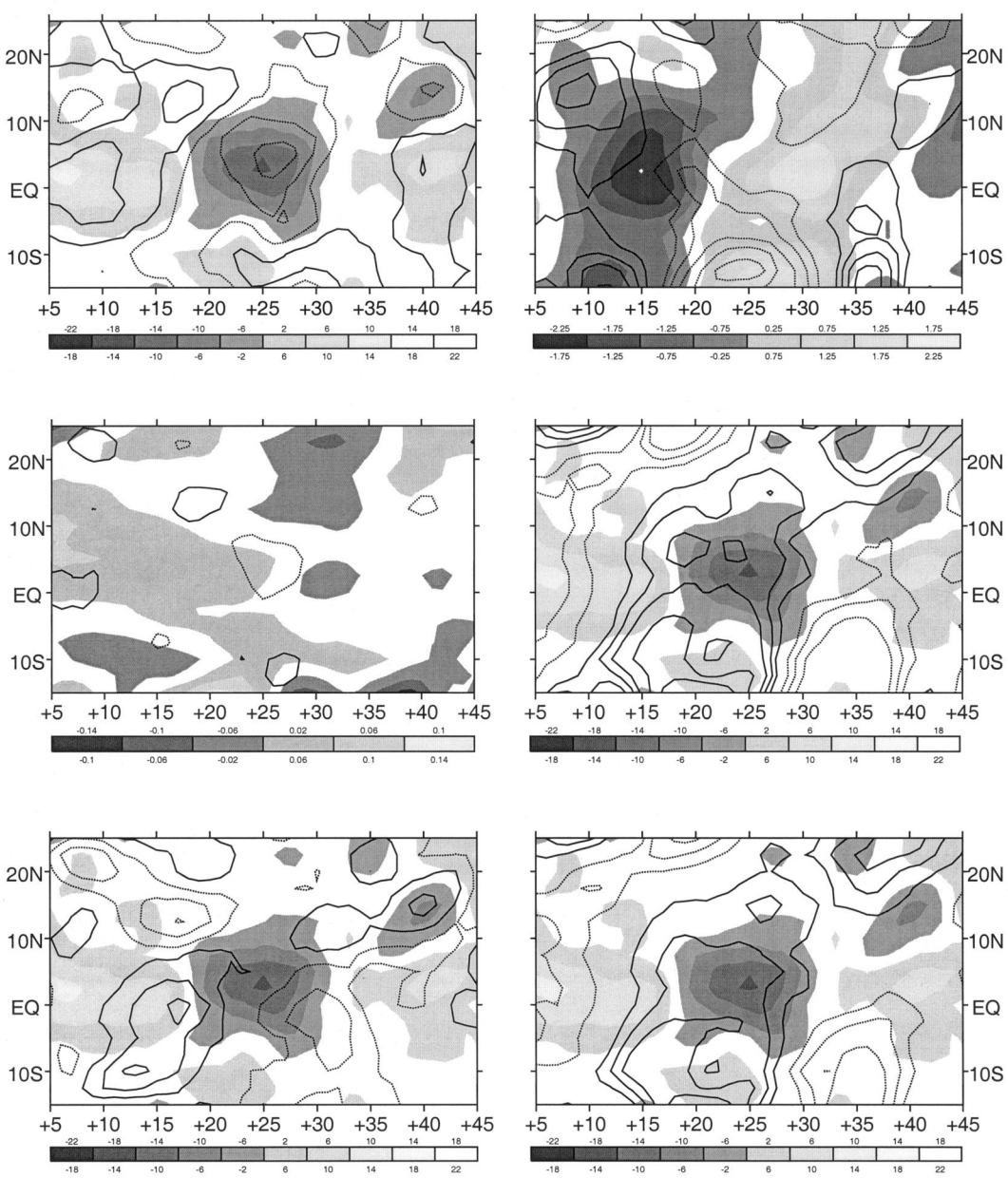

FIG. 10. May–Jun Hovmoeller diagram for 125°–170°E. Abscissa, grayscale, and contours as in Fig. 9.

waves are emitted by equatorial convection in MJ, but they are much weaker, and the northern lobe, while detectable from day +15 to day +30, does not amplify enough to appear in Fig. 10 until it reaches 8°N. The bulk of the enhanced and suppressed convective signal in MJ occurs near the equator. The positive skin temperature anomaly moves into the western Pacific from the northwest along with the positive ω(500 mb) and DSWRF anomalies (Fig. 10b). There is no northward propagation of the positive DSWRF or skin temperature anomalies in MJ, although a weak northward-moving negative ω(500 mb) anomaly is visible. Most of the signal in the 850-mb zonal wind anomaly is concentrated around the equator, unlike AO, in which the negative (positive) anomalies move northward leading (lagging) the convection. The basic pattern of positive DSWRF and surface temperature anomaly and enhanced flux of moisture out of the ocean into the atmosphere leading the convective anomaly in the direction of its propagation has been noted for the MJO by Shinoda et al. (1998), Zhang (1996), Hendon and Glick (1997), and, most recently, Woolnaugh et al. (2000), among others. For the northward propagation in the Indian Ocean in the BSISO, both AO and MJ echo this MJO pattern.

Air–sea interaction in the latter half of the AO BSISO

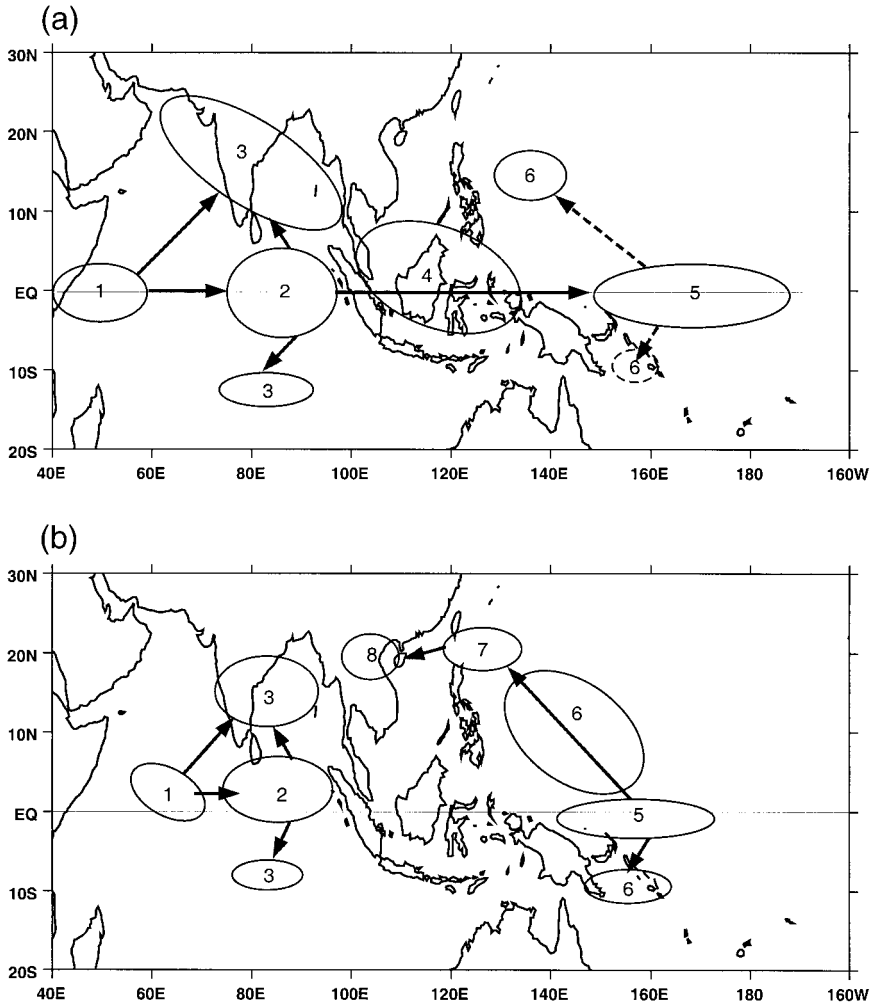

FIG. 11. BSISO convection life cycle schematic for (a) May–Jun and (b) Aug–Oct. Ovals indicate convection, with numbers indicating the evolution of the anomaly. Black arrows indicate eastward propagation of convection along or near the equator. Gray arrows indicate poleward propagation of convection due to emanation of Rossby waves from equatorial convection. Dashed lines indicate low-amplitude signal.

cycle in the western Pacific is similar to that of both MJ and AO in the Indian Ocean. In all three cases, equatorial convection emits a Rossby wave and the growth of the northern lobe is favored over the southern lobe by the highly asymmetric distribution of the vertical wind shear and low-level moisture distributions. The evolution of the suppressed convective phase prior to the onset of the convection determines the pattern of the air–sea interaction. Figure 10 shows that the MJ equatorial mode is favored by a pattern of suppression and SST buildup that is strongest along the equator. In AO, the northward-propagating Rossby wave emitted by suppressed equatorial convection during day -5 to day 0 creates a pattern of positive DSWRF, SST, and latent heat flux anomalies that encourage the northward-propagating mode rather than an equatorial one. These results suggest that air–sea interaction plays a role in amplifying the BSISO but does not determine its structure.

6. Summary and discussion

In this study, we have examined the structure of the BSISO with the intent of understanding its underlying physics, and providing an observational framework for the evaluation of climate models. Our results show that there are significant differences between the early and late boreal summer ISO, and that Rossby waves play a critical role in its structure. We also find evidence of air–sea interaction.

a. Summary of BSISO life cycle

Figure 11 is a schematic of the composite MJ and AO BSISO life cycles and serves as a summary of the

results of this study. Stages 1–3 show initiation and eastward propagation of the MJ and AO BSISO convective anomaly in the Indian Ocean, followed by emission of poleward-moving Rossby waves. The transition of convection from the Indian Ocean to the western Pacific occurs at stage 4. Rossby waves are emitted from convection in the equatorial western Pacific at stage 5 and travel poleward during stage 6 (and 7 and 8 for AO). Dissipation of the current cycle occurs after stage 6 (8) for MJ (AO).

There are several important differences between the MJ and AO life cycles. The first is the initial formation of the convective anomaly in the Indian Ocean. In the MJ composite, the convective anomaly at day −5 is centered in the western Indian Ocean (Fig. 4b), while for the AO case, the convection at this stage is most intense in the central and eastern Indian Ocean (Fig. 5b). Convection and circulation anomalies are stronger and more extensive in MJ than in AO; in MJ, the convection is more symmetric about the equator during day −10 to day 0, while in AO, it is located largely north of the equator.

During the middle of the cycle, the main difference is that convection in MJ shows continuous propagation along the Maritime Continent, while AO undergoes a discrete jump of convection from the Indian Ocean to the western Pacific. During the latter part of the BSISO cycle, the life cycles diverge dramatically, with AO showing intense coherent northwestward-propagating anomalies of circulation and convection in the western Pacific, while the MJ composite exhibits dominant eastward propagation along the equator on the western Pacific and far weaker northwestward-propagating anomalies.

Our results highlight the importance of the seasonal cycle to the character of the ISO as suggested by Slingo et al. (1996), Wang and Xie (1997), and LW. It has been noted that ISO convection tends to follow the seasonal march of the region of climatologically favored convection (Salby and Hendon 1994; Li and Wang 1994). Near the equinoxes, the thermal equator lies near the geographic equator, and ISO convection tends to move along the equator, exciting the moist Kelvin–Rossby wave mode and frictional wave–CISK-type interactions. The Rossby waves associated with the convection are symmetric about the equator. With the onset of boreal summer, the region of maximum OLR variance moves northward into the Asian monsoon region and the northern west Pacific, and the path followed by ISO convection shifts along with it. This affects the character of the ISO in both the Indian and Pacific Ocean basins.

In the Indian Ocean, the equatorial mode seen in winter is still present in MJ, but the summertime distribution of SSTs, low-level moisture, and wind shear favors the movement of convection to the north. Rossby waves generated by the equatorial ISO convection become highly asymmetric, with the northern lobe strongly favored. The MJ ISO accordingly shows pronounced northward propagation in the Asian monsoon region; this northward propagation is absent in winter. In AO, a region of easterly shear still occupies the northern and central Indian Ocean, favoring the northern Rossby lobe, but the low-level moisture and SSTs are reduced relative to MJ. The region of climatologically favored convection shifts farther northward of the equator, so that the eastward-propagating equatorial mode is weaker in AO than in MJ. The result of these changes in boundary conditions is that the AO BSISO in the Indian Ocean is similar to that of MJ, but weaker in amplitude.

In the western Pacific, by the time of AO, the regions of maximum SST and low-level moisture (Figs. 2c,d) have moved well north of the equator, and the region of easterly vertical wind shear has intensified and extended farther into the western Pacific relative to MJ. Convection is favored to the north of the equator. The eastward-moving equatorially trapped Kelvin–Rossby wave mode is suppressed, and the northwestward-propagating Rossby mode is favored. The MJ case lies somewhere in between that of AO and boreal winter. Both northward-moving and eastward-moving modes are evident in MJ in the western Pacific. Eastward-moving convection along the equator is dominant but is substantially weaker than during the equinoxes, and some northwestward propagation in the western Pacific is evident.

b. Air–sea interaction in the BSISO

Coherent propagation of anomalies of skin temperature, latent heat flux, and DSWRF along with the convection suggest that air–sea interactions accompany the BSISO. For both AO and MJ, interaction between the ocean surface and the overlying air plays a role in generating the instability necessary for convection. Figure 12 depicts the northward propagation of convection in the Indian Ocean for MJ and in the western Pacific for AO. The figure is oriented along a section of the Indian Ocean or western Pacific (southwest–northeast for MJ and southeast–northwest for AO). The solid vertical arrows represent rising motion within the convective anomaly and subsidence to its north and south. Subsidence to the north of the convection creates an area of clear skies and allows a positive DSWRF anomaly to form. The positive DSWRF anomaly heats the earth's surface, causing a positive skin temperature anomaly. The positive skin temperature creates low pressure at the surface, and low-level convergence begins. Meanwhile, the positive skin temperature anomaly and the arrival of strong easterly wind anomalies create conditions favorable for the development of a negative latent heat flux anomaly. The negative latent heat flux anomaly and the low-level convergence increase the low-level moisture, causing a positive h(1000 mb) anomaly to form. The atmosphere is destabilized, and convection moves farther northward.

As convection arrives over a given location, the cloud

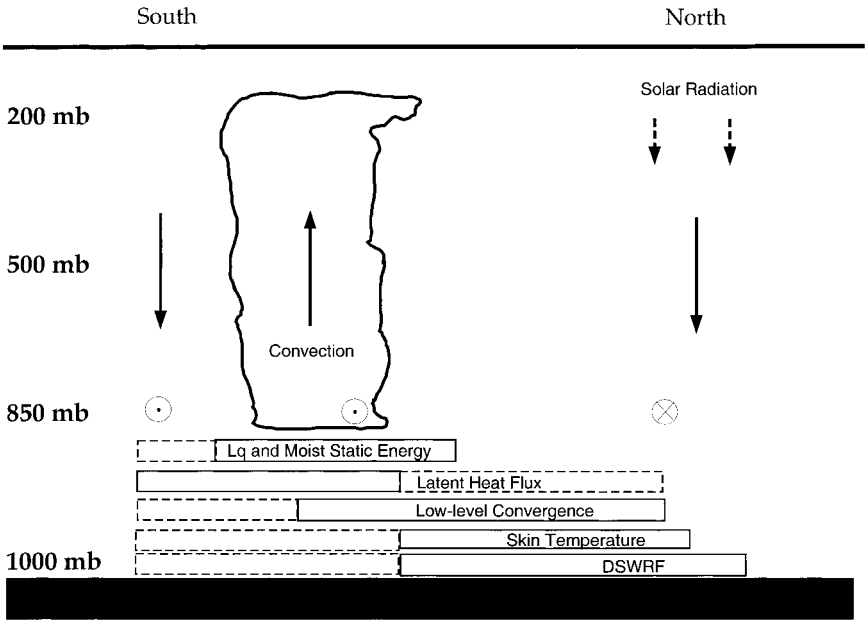

FIG. 12. Schematic of air–sea interaction in the northward propagation of convective anomalies associated with the BSISO in the Indian and western Pacific Oceans. Dark vertical lines indicate the ω(500 mb) anomaly. The cloud indicates deep precipitating convection. The boxes represent the approximate locations of anomalies relative to the convection. Solid box indicates a positive anomaly, and dashed box indicates a negative anomaly. Circles indicate direction of 850-mb zonal wind anomaly with the $\otimes$ ($\odot$) representing easterlies (westerlies).

cover causes the DSWRF anomaly to go from positive to negative, and the skin temperature soon follows suit. With the onset of the low-level westerly winds that accompany the convection, the latent heat flux anomaly goes from negative to positive. Low-level convergence changes to divergence, and the moist static energy drops, as moisture is transported out of the boundary layer and into the troposphere by convection.

7. Conclusions

The results of this study show that the simulation of the BSISO is a rigorous test for general circulation models. To reproduce both AO and MJ cases with fidelity, a GCM must simulate the seasonal changes in the mean flow and reproduce westward-moving wave activity as well as air–sea interactions. Because of the strong evidence here for the existence of air–sea interaction in the BSISO, this study suggests that coupled models may be necessary to reproduce the intraseasonal variability in the Asian monsoon region. Modeling studies are needed to determine how the surface flux and wind anomalies work together to foster the propagation of convection and are currently being carried out.

Although this study has described the basic structure of the BSISO, it leaves a number of important questions unanswered. More work is needed to further understand the reasons for the northward propagation of convection in the BSISO and the discrete jump of convection from the Indian Ocean to the western Pacific in AO. Other unresolved issues include the reasons why the anomalous convection at intraseasonal timescales tends to form large-scale coherent anomalies, why the Indian Ocean is a region of strong ISO convective variance throughout the year, and why the periodicity of the BSISO is shorter than that of its boreal winter counterpart.

Acknowledgments. NCEP–NCAR reanalysis data were provided by the NOAA–CIRES Climate Diagnostics Center, Boulder, Colorado, from their Web site at http://www.cdc.noaa.gov. This research was supported by the Climate Dynamics Program, National Science Foundation under Grant ATM 96-13776. This is School of Ocean and Earth Science and Technology (SOEST) Publication 5485.

REFERENCES

Chen, T.-C., and M. Murakami, 1988: The 30–50 day variation of convective activity over the western Pacific Ocean with emphasis on the northwestern region. *Mon. Wea. Rev.*, **116,** 892–906.

Flatau, M., P. J. Flatau, P. Phoebus, and P. P. Niiler, 1997: The feedback between equatorial convection and local radiative and evaporative processes: The implications for intraseasonal oscillations. *J. Atmos. Sci.*, **54,** 2373–2386.

Gill, A. E., 1980: Some simple solutions for heat induced tropical circulation. *Quart. J. Roy. Meteor. Soc.*, **106,** 447–463.

Graham, N., and T. P. Barnett, 1987: Observations of sea surface temperature and convection over tropical oceans. *Science,* **238,** 657–659.

Hartmann, D. L., and M. L. Michelsen, 1989: Intraseasonal periodicities in Indian rainfall. *J. Atmos. Sci.,* **46,** 2838–2862.

——, ——, and S. A. Klein, 1992: Seasonal variations of tropical intraseasonal oscillations: A 20–25-day oscillation in the western Pacific. *J. Atmos. Sci.,* **49,** 1277–1289.
Hendon, H. H., and M. L. Salby, 1994: The life cycle of the Madden–Julian oscillation. *J. Atmos. Sci.,* **51,** 2225–2237.
——, and J. Glick, 1997: Intraseasonal air–sea interaction in the tropical Indian and Pacific Oceans. *J. Climate,* **10,** 647–661.
Hoskins, B. J., and M. J. Rodwell, 1995: A model of the Asian summer monsoon. Part I: The global scale. *J. Atmos. Sci.,* **52,** 1329–1340.
Jones, C., and B. C. Weare, 1996: The role of low-level moisture convergence and ocean latent heat fluxes in the Madden and Julian oscillation: An observational analysis using ISCCP data and ECMWF analyses. *J. Climate,* **9,** 3086–3104.
——, D. E. Waliser, and C. Gautier, 1998: The influence of the Madden–Julian oscillation on ocean surface heat fluxes and sea surface temperature. *J. Climate,* **11,** 1057–1072.
Kalnay, E., and Coauthors, 1996: The NCEP/NCAR 40-Year Reanalysis Project. *Bull. Amer. Meteor. Soc.,* **77,** 437–471.
Kemball-Cook, S. R., and B. C. Weare, 2001: The onset of convection in the Madden–Julian oscillation. *J. Climate,* **14,** 780–793.
Krishnamurti, T. N., and D. Subrahmanyam, 1982: The 30–50 day mode at 850 mb during MONEX. *J. Atmos. Sci.,* **39,** 2088–2095.
——, D. K. Oosterhof, and A. V. Mehta, 1988: Air–sea interaction on the time scale of 30 to 50 days. *J. Atmos. Sci.,* **45,** 1304–1322.
Krishnan, R., C. Zhang, and M. Sugi, 2000: Dynamics of breaks in the Indian summer monsoon. *J. Atmos. Sci.,* **57,** 1354–1372.
Lau, K.-H., and N.-C. Lau, 1990: Observed structure and propagation characteristics of tropical summertime synoptic scale disturbances. *Mon. Wea. Rev.,* **118,** 1888–1913.
Lau, K.-M., and C.-H. Sui, 1997: Mechanisms of short-term sea surface temperature regulation: Observations during TOGA COARE. *J. Climate,* **10,** 465–472.
Li, T., and T. F. Hogan, 1999: The role of the annual-mean climate on seasonal and interannual variability of the tropical Pacific in a coupled GCM. *J. Climate,* **12,** 780–792.
——, and B. Wang, 1994: The influence of sea surface temperature on the tropical intraseasonal oscillation: A numerical experiment. *Mon. Wea. Rev.,* **122,** 2349–2362.
Liebmann, B., and C. A. Smith, 1996: Description of a complete (interpolated) OLR dataset. *Bull. Amer. Meteor. Soc.,* **77,** 1275–1277.
Lin, X., and R. H. Johnson, 1996: Kinematic and thermodynamic characteristics of the flow over the western Pacific warm pool during TOGA COARE. *J. Atmos. Sci.,* **53,** 695–715.
Madden, R. A., 1986: Seasonal variations of the 40–50 day oscillation in the Tropics. *J. Atmos. Sci.,* **43,** 3138–3158.
——, and P. R. Julian, 1971: Detection of a 40–50 day oscillation in the zonal wind in the tropical Pacific. *J. Atmos. Sci.,* **28,** 702–708.
——, and ——, 1972: Description of global-scale circulation cells in the Tropics with a 40–50 day period. *J. Atmos. Sci.,* **29,** 1109–1123.
——, and ——, 1994: Observations of the 40–50-day tropical oscillation—a review. *Mon. Wea. Rev.,* **122,** 814–883.
Maloney, E. D., and D. L. Hartmann, 1998: Frictional moisture convergence in a composite life cycle of the Madden–Julian oscillation. *J. Climate,* **11,** 2387–2403.
Matsuno, T., 1966: Quasi-geostrophic motions in the equatorial area. *J. Meteor. Soc. Japan,* **44,** 25–42.
Mechoso, C. R., and Coauthors, 1995: The seasonal cycle over the tropical Pacific in coupled ocean–atmosphere general circulation models. *Mon. Wea. Rev.,* **123,** 2825–2838.
Murakami, T., T. Nakazawa, and J. He, 1984: On the 40–50 day oscillations during the 1979 Northern Hemisphere summer I: Phase propagation. *J. Meteor. Soc. Japan,* **62,** 440–468.
Nitta, T., 1987: Convective activities in the tropical western Pacific and their impacts on the Northern Hemisphere summer circulation. *J. Meteor. Soc. Japan,* **65,** 165–171.
Press, W. H., S. A. Teukolsky, W. T. Vetterling, and B. P. Flannery, 1986: *Numerical Recipes.* Cambridge University Press, 848 pp.
Rui, H., and B. Wang, 1990: Development characteristics and dynamic structure of tropical intraseasonal convection anomalies. *J. Atmos. Sci.,* **47,** 357–379.
Salby, M. L., and H. H. Hendon, 1994: Intraseasonal behavior of clouds, temperature, and motion in the Tropics. *J. Atmos. Sci.,* **51,** 2207–2224.
Shinoda, T., and H. H. Hendon, 1998: Mixed layer modeling of intraseasonal variability in the tropical western Pacific and Indian Oceans. *J. Climate,* **11,** 2668–2685.
——, ——, and J. Glick, 1998: Intraseasonal variability of surface fluxes and sea surface temperature in the tropical western Pacific and Indian Oceans. *J. Climate,* **11,** 1685–1702.
Slingo, J. M., and Coauthors, 1996: The intraseasonal oscillation in 15 atmospheric general circulation models: Results from an AMIP diagnostic subproject. *Climate Dyn.,* **12,** 325–357.
Waliser, D. E., K.-M. Lau, and J.-H. Kim, 1999: The influence of coupled sea surface temperatures on the Madden–Julian oscillation: A model perturbation experiment. *J. Atmos. Sci.,* **56,** 333–358.
Wang, B., and H. Rui, 1990: Synoptic climatology of transient tropical intraseasonal convection anomalies: 1975–1985. *Meteor. Atmos. Phys.,* **44,** 43–61.
——, and X. Xie, 1996: Low-frequency equatorial waves in vertically sheared zonal flow. Part I: Stable waves. *J. Atmos. Sci.,* **53,** 449–467.
——, and ——, 1997: A model for the boreal summer intraseasonal oscillation. *J. Atmos. Sci.,* **54,** 72–86.
——, and ——, 1998: Coupled modes of the warm pool climate system: Part I: The role of air–sea interaction in maintaining the Madden–Julian oscillation. *J. Climate,* **11,** 2116–2135.
Webster, P. J., and Coauthors, 1998: Processes, predictability, and the prospects for prediction. *J. Geophys. Res.,* **103,** 14 451–14 510.
Wheeler, M., and G. N. Kiladis, 1999: Convectively coupled equatorial waves: Analysis of clouds and temperature in the wavenumber–frequency domain. *J. Atmos. Sci.,* **56,** 374–399.
Woolnaugh, S. J., J. M. Slingo, and B. J. Hoskins, 2000: The relationship between convection and sea surface temperature on intraseasonal timescales. *J. Climate,* **13,** 2086–2104.
Xie, X., and B. Wang, 1996: Low-frequency equatorial waves in vertically sheared zonal flow. Part II: Unstable waves. *J. Atmos. Sci.,* **53,** 3589–3605.
Yasunari, T., 1979: Cloudiness fluctuations associated with the Northern Hemisphere summer monsoon. *J. Meteor. Soc. Japan,* **57,** 227–242.
Zhang, C., 1996: Atmospheric intraseasonal variability at the surface in the tropical western Pacific Ocean. *J. Atmos. Sci.,* **53,** 739–758.
Zhu, B., and B. Wang, 1993: The 30–60-day convection seesaw between the tropical Indian and western Pacific Oceans. *J. Atmos. Sci.,* **50,** 184–199.